Figure S1, associated with figure 1

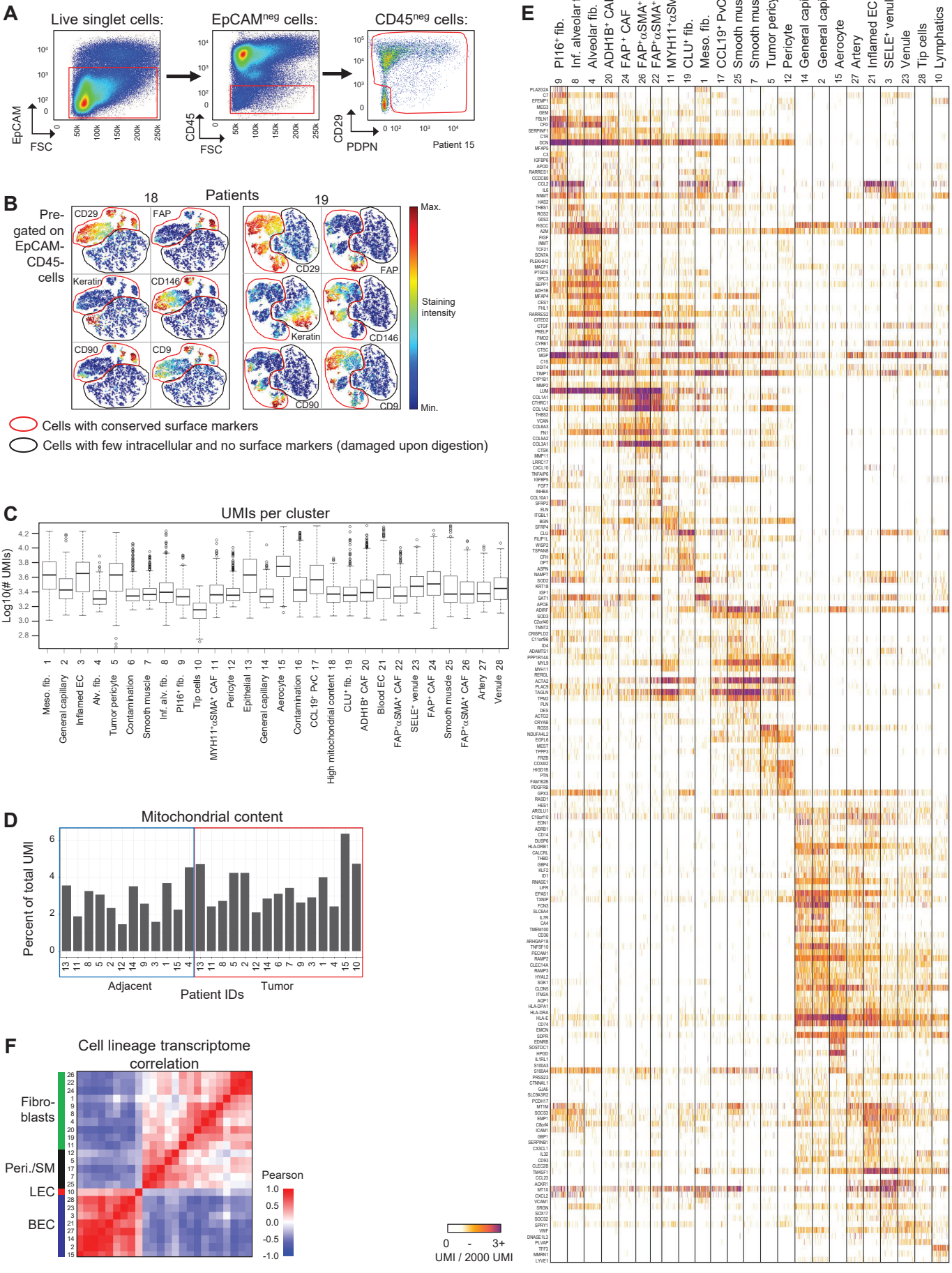

Supplemental fig. 1 (related to fig. 1) | A, Flow cytometry sorting strategy to enrich for stromal cells. EpCAM and CD45 gating removed epithelial and immune cell populations, respectively. Integrin β1 (CD29) and podoplanin (PDPN) positive gating was used to remove any remaining damaged cell that lost surface markers upon tissue digestion (as seen in Fig. S1B). **B**, CyTOF viSNE representation of pre-gated cisplatin^{neg} (for dead cell exclusion) EpCAM^{neg} CD45^{neg} cells obtained from tumor lesions of two NSCLC patients (#18 and 19). The two viSNE plots show a substantial cell cluster (circled in black) lacking the 15 surface markers in the CyTOF antibody panel (here, 5 surface markers – CD29, FAP, CD146, CD90, CD9 – are shown as representative examples), while preserving levels of intracellular markers (such as keratin and vimentin). These results indicate that these cells likely contain live but damaged cells that lost surface protein expression upon tissue digestion (potentially tumor, immune, or stromal damaged cells). They could also contain red blood cells. Notably, all remaining cells expressed CD29, which was therefore selected as a positive marker including all undamaged stromal cells. **C**, Boxplot of UMI counts per scRNAseq cluster. **D**, Mitochondrial gene content for all sequenced cells in the tumor and its adjacent stroma for each patient. **E**, Highly variable genes across all stromal clusters. Genes were selected if they were highly variable (Log2(var/mean) = 1.25) and met a minimum expression cutoff of 8 UMI across all cells included. **F**, Heatmap showing the correlation (Pearson) between whole genome expression profiles of major stromal populations. Fibroblast, perivascular, and endothelial lineages show high concordance as expected. Gene expression values per cluster are determined by taking the mean expression of each gene across all cells then taking the log2 value.

Figure S2, associated with figure 1

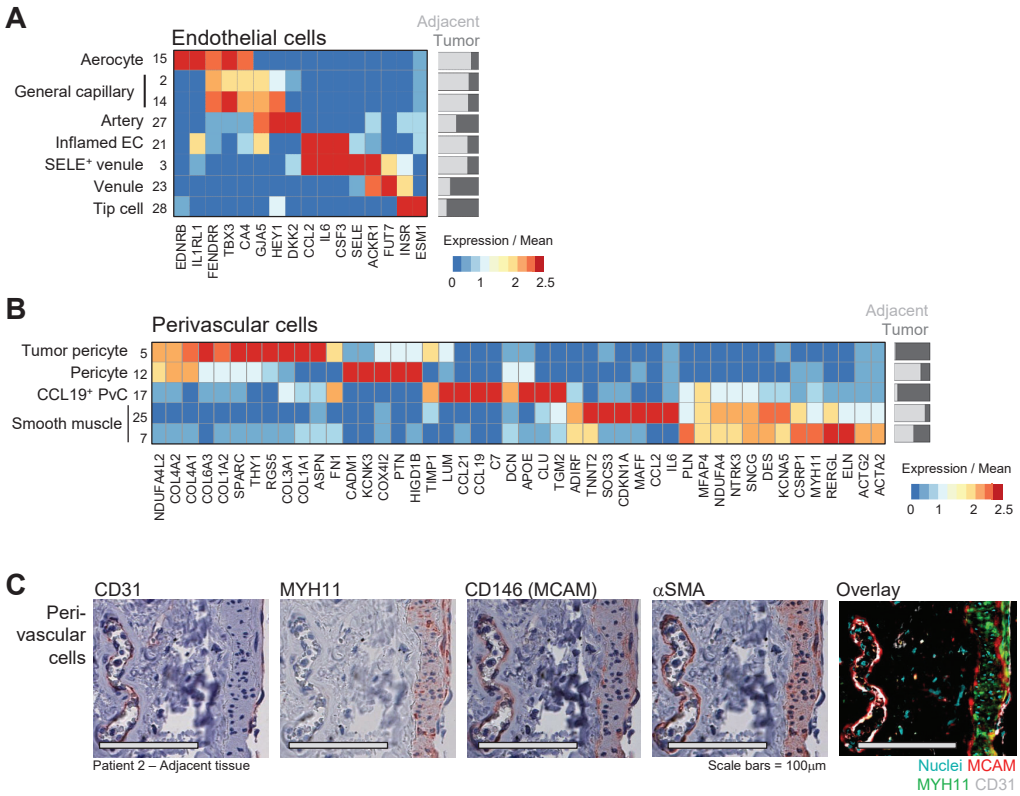

Supplemental fig. 2 (related to fig. 1) | A-B, (**A**) Gene lists highlighting identifying genes and heterogeneity between EC clusters and (**B**) PvC clusters. **C**, IHC staining of blood vessel showing pericytes (CD146 and αSMA), smooth muscle cells (CD146, αSMA and MYH11) and ECs (CD146 and CD31). All scale bars are 100μm.

Figure S3, associated with figure 1

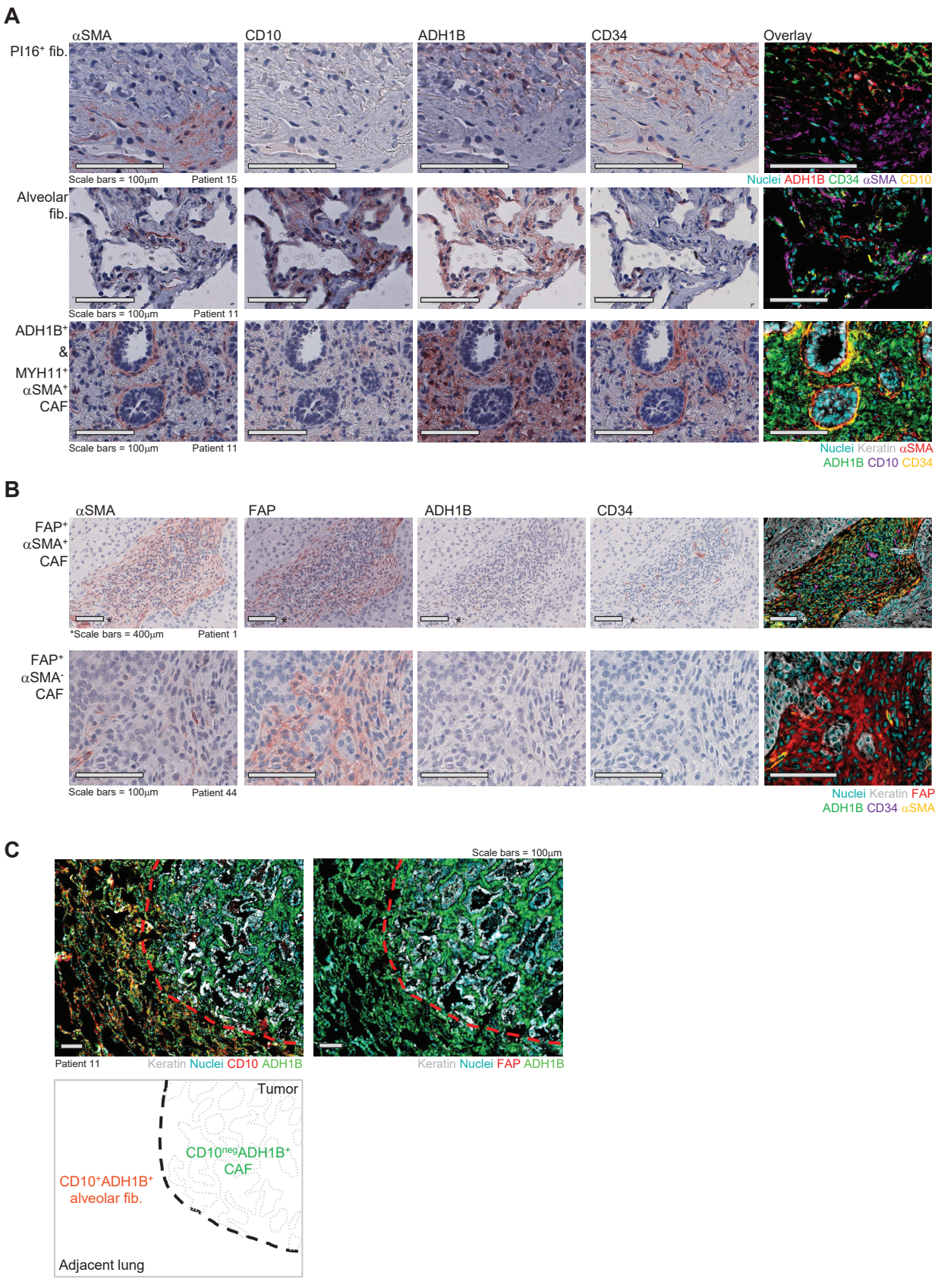

Supplemental fig. 3 (related to fig. 1) | (**A**), IHC stains highlighting PI16^{+} fib., alv. fib., ADH1B^{+} CAF and MYH11^{+}αSMA^{+} CAF. All scale bars are 100μm. (**B**), IHC staining of FAP^{+} CAF highlighting heterogeneity within this fibroblast subset demonstrated by αSMA intensity. FAP^{+} CAF (top panels) scale bars are 100μm and FAP^{+}αSMA^{+} CAF scale bars are 400μm. **C**, Multiplexed IHC highlighting lack of FAP and CD10 staining in ADH1B^{+} CAF cells. All scale bars are 100μm.

Figure S4, associated with figure 3

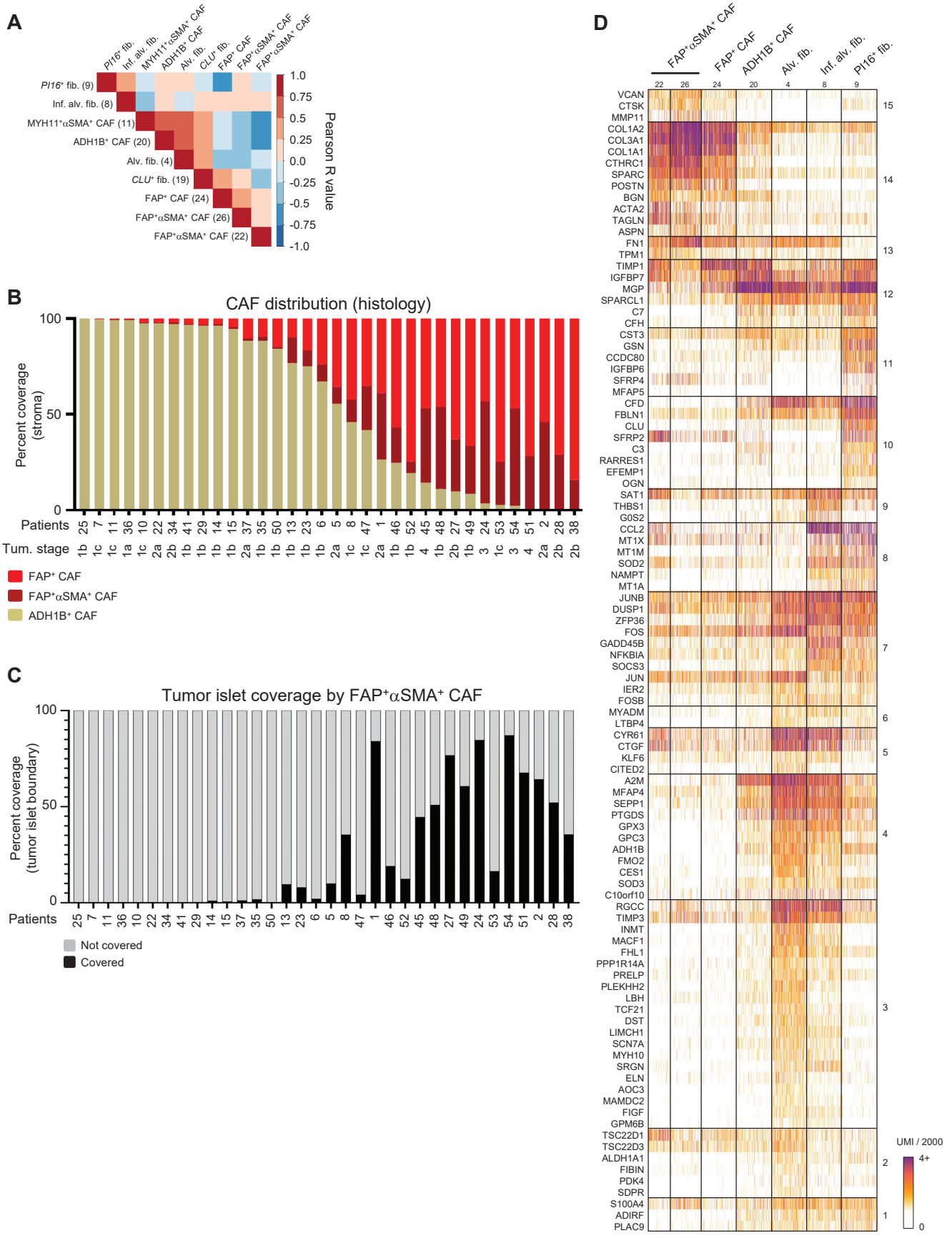

Supplemental fig. 4 (related to fig. 3) | A, Correlation (Pearson) of fibroblast subset abundance in scRNAseq tumor samples. **B**, Co-expressed gene 'modules' identified within the fibroblast clusters. Each module contains a group of genes with highly correlated expression regardless of enrichment in any particular cluster. These modules frequently represent identifying genes for specific clusters, such as modules 14 and 15 for FAP^+ CAF, but may also represent groups of genes co-regulated across multiple clusters, like module 7. Genes were selected if they were highly variable (Log2(var/mean) = 0.9) and met a minimum expression cutoff of 10 UMI across all cells included. **C**, Mean log10 gene expression of $PI16^+$ fib., alv. fib. and FAP^+ CAF-associated gene modules displayed by density histogram. Higher peaks indicate greater cell numbers at the expression level indicated on the X axis. Single-cell gene expression of modules is shown in Figure S4B. **D**, Correlation (Pearson) of $ADH1B^+$ CAF and FAP^+ CAF gene signature components in TCGA.

Figure S5, associated with figure 3

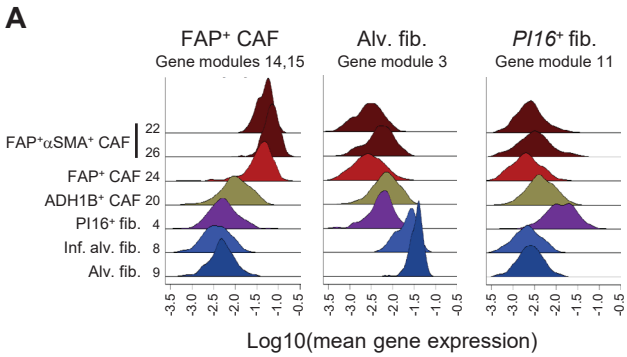

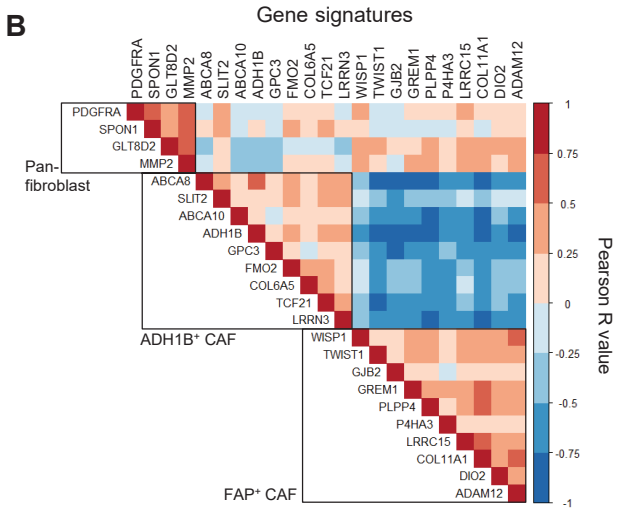

Supplemental fig. 5 (related to fig. 3) | A, ADH1B^{+}, FAP^{+} and FAP^{+}αSMA^{+} CAF coverage across IHC samples highlighting differential CAF enrichment between patients. **B**, FAP^{+}αSMA^{+} CAF coverage on tumor islets.

Figure S6 associated with figure 3

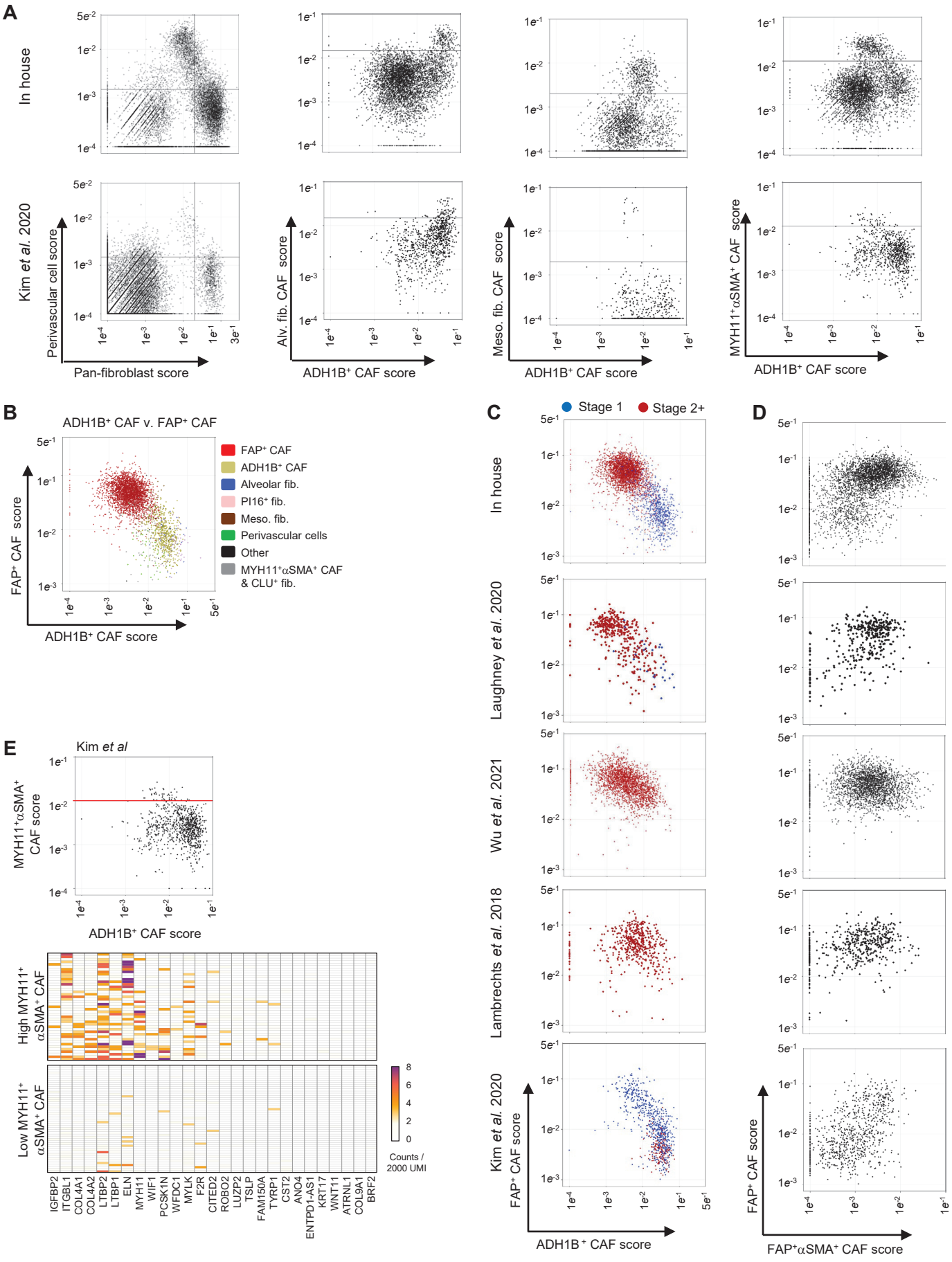

Supplemental fig. 6 (related to fig. 3) | Confirmation of $ADH1B^+$ and FAP^+ CAF in external NSCLC scRNAseq datasets. **A**, Fibroblasts were initially isolated from other cells using positive gating for fibroblasts and negative gating against perivascular cells. Then, alv. fib., meso. fib., and $MYH11^+\alpha SMA^+$ CAF were isolated and removed sequentially. This is shown for our in house dataset and a representative external dataset (24). **B**, The remaining cells are colored by their cluster IDs and plotted against the $ADH1B^+$ and FAP^+ CAF gene scores. **C**, Cells are colored by the tumor stage of the sample they come from and again plotted against the $ADH1B^+$ and FAP^+ CAF gene scores. **D,** A scatterplot showing FAP^+ by $FAP^+\alpha SMA^+$ CAF gene scores. **E,** (top) Expression of $MYH11^+\alpha SMA^+$ CAF gene score versus ADH1B+ gene scores. A red line depicts the cutoff used to define $MYH11^+\alpha SMA^+$ CAF low gene score cells. (bottom) Expression of $MYH11^+\alpha SMA^+$ CAF genes in low and high gene score cells.

Figure S7 associated with figure 3

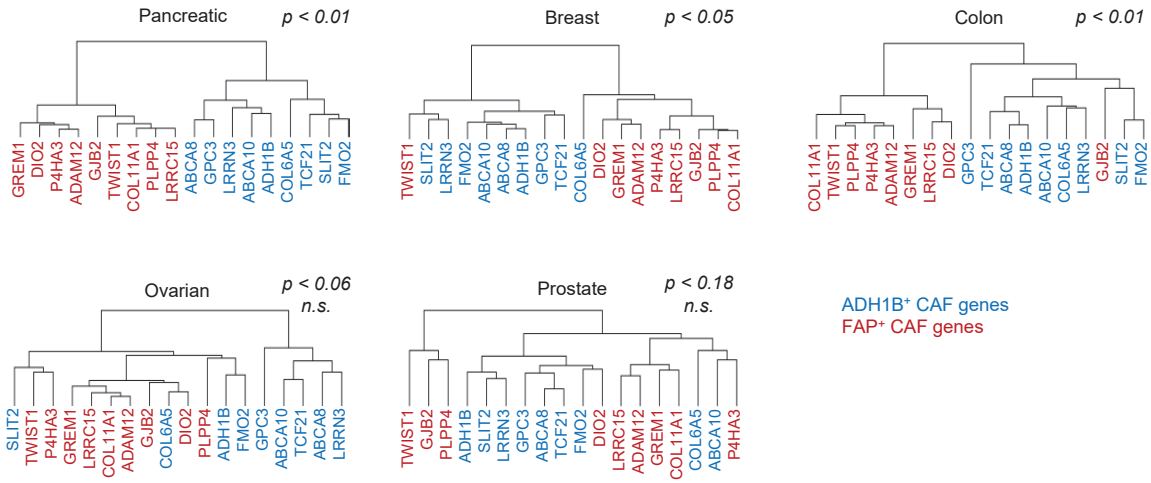

Supplemental fig. 7 (related to fig. 3) | A, ADH1B^{+} and FAP^{+} CAF gene signature presentation in other tumor types. Dendrogram visualization of hierarchical clustering of our ADH1B^{+} and FAP^{+} CAF gene signatures. P values are the chi-square significance of the co-assignment of signatures genes into the same group in the two main subtrees.

Figure S8, associated with figure 4

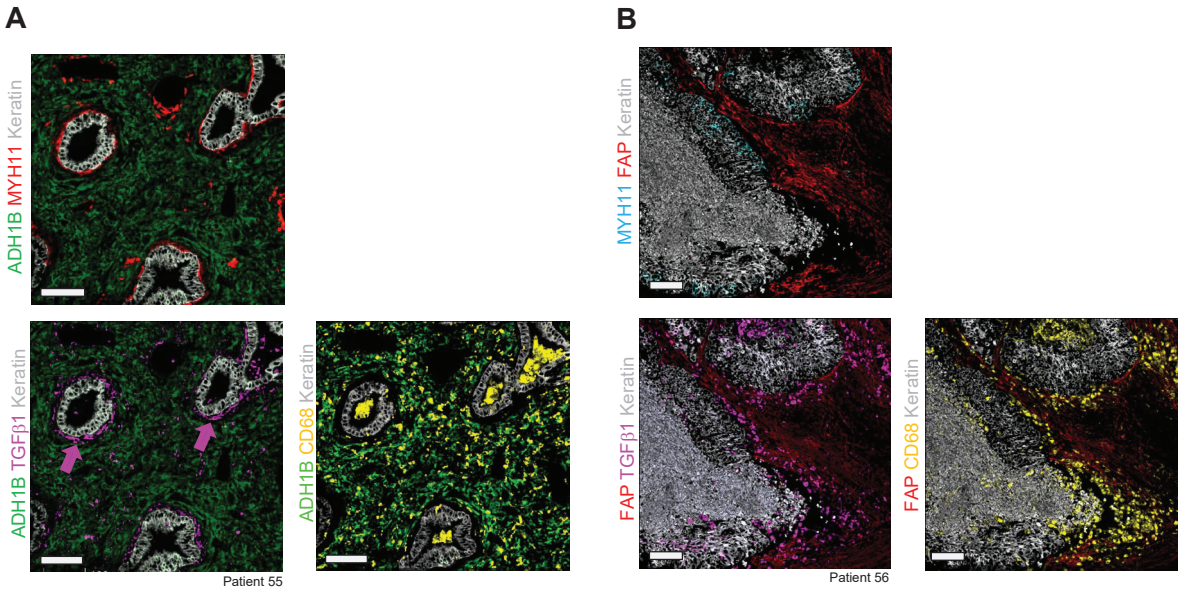

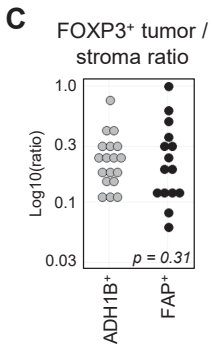

Supplemental fig. 8 (related to fig. 4) | A, (left panels) TGFβ1 staining is co-localized with MYH11 at the tumor border and supports the observed expression of TGFB1 in $MYH11^{+}\alpha SMA^{+}$ CAF as seen in figure 4A. (right panel) As a positive confirmation of TGFβ1 specificity, staining is seen co-localized with some $CD68^{+}$ alveolar macrophages as expected based on prior literature (74). **B**, TGFβ1 staining is not found co-localized with FAP^{+} CAF, confirming the specificity of TGFβ1 to $MYH11^{+}\alpha SMA^{+}$ CAF as observed in the expression data. **C**, IHC quantification of the tumor / stroma $FOXP3^{+}$ cells per mm^2 ratio. Tumor samples are stratified by their stroma profile ($ADH1B^{+}$ CAF rich or FAP^{+} CAF rich) and no significant difference was observed.

1. Yu X, Buttgereit A, Lelios I, Utz SG, Cansever D, Becher B, et al. The Cytokine TGF-β Promotes the Development and Homeostasis of Alveolar Macrophages. Immunity. 2017;47:903-912.e4.

Figure S9, associated with figure 5

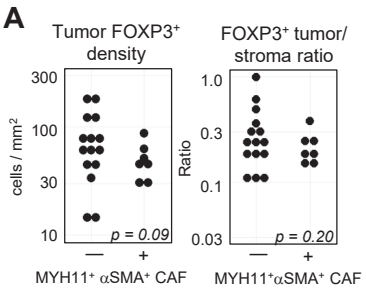

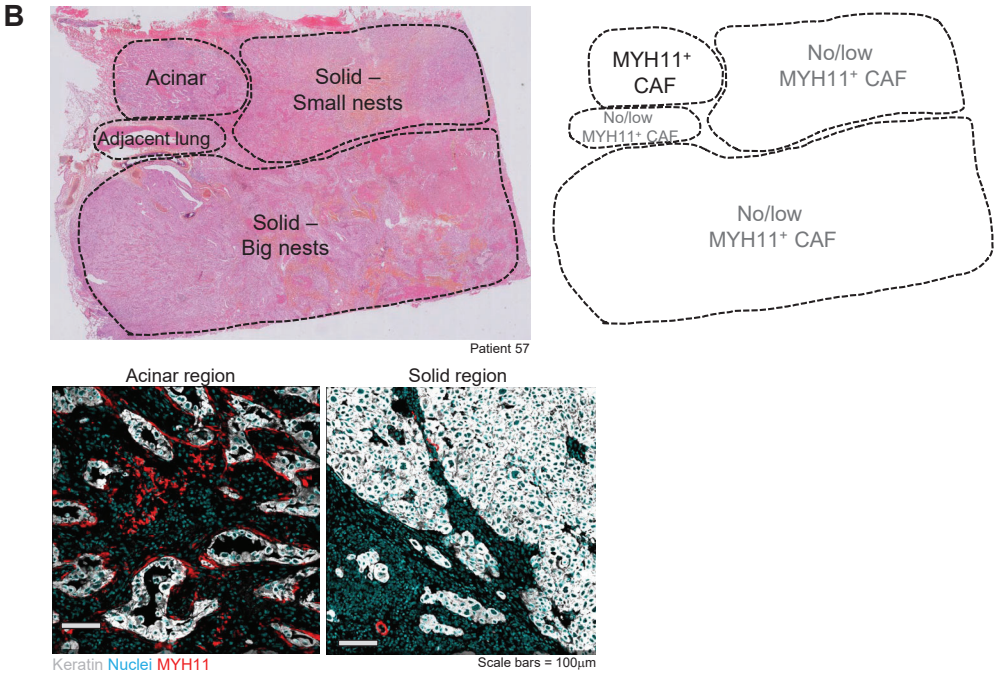

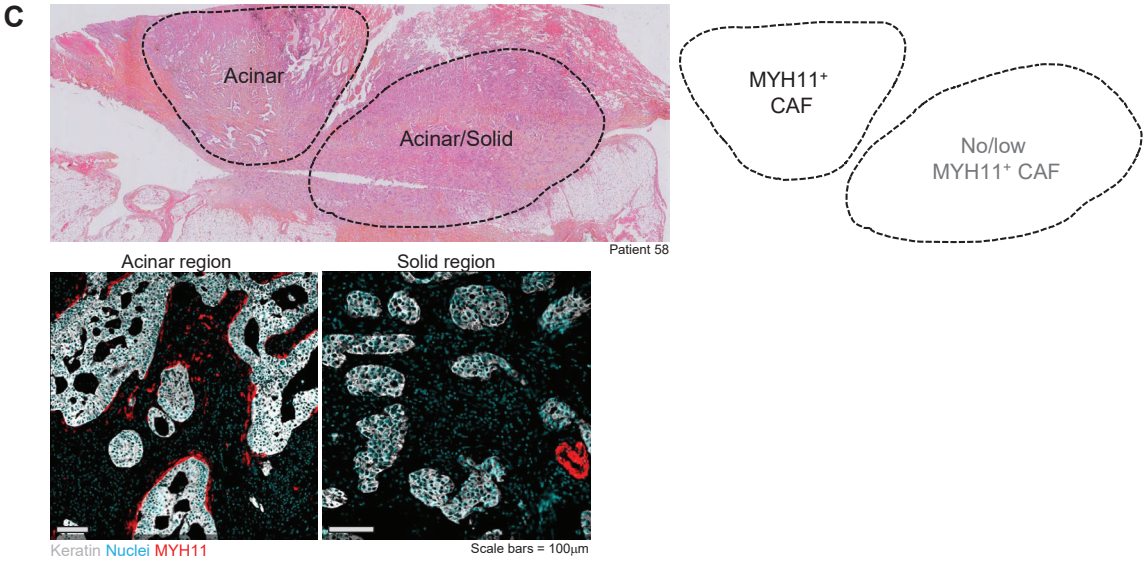

Supplemental fig. 9 (related to fig. 5) | A, The presence or absence of $MYH11^{+}\alpha SMA^{+}$ CAF shows no significant differences (t test) in tumor infiltrating $FOXP3^{+}$ cells per mm^2 (left) and the ratio of $FOXP3^{+}$ cells per mm^2 in the tumor versus stroma (right). Only early stage (tumor stage 1) patients were included to eliminate bias due to $MYH11^{+}\alpha SMA^{+}$ CAF rarely being found at later stage. **B & C**, IHC staining of MYH11 and keratin highlights $MYH11^{+}\alpha SMA^{+}$ CAF preferential enrichment for acinar versus solid pathologies, in tumor samples harboring histological subtypes heterogeneity, as labeled by a pathologist.

Figure S10, associated with figure 5

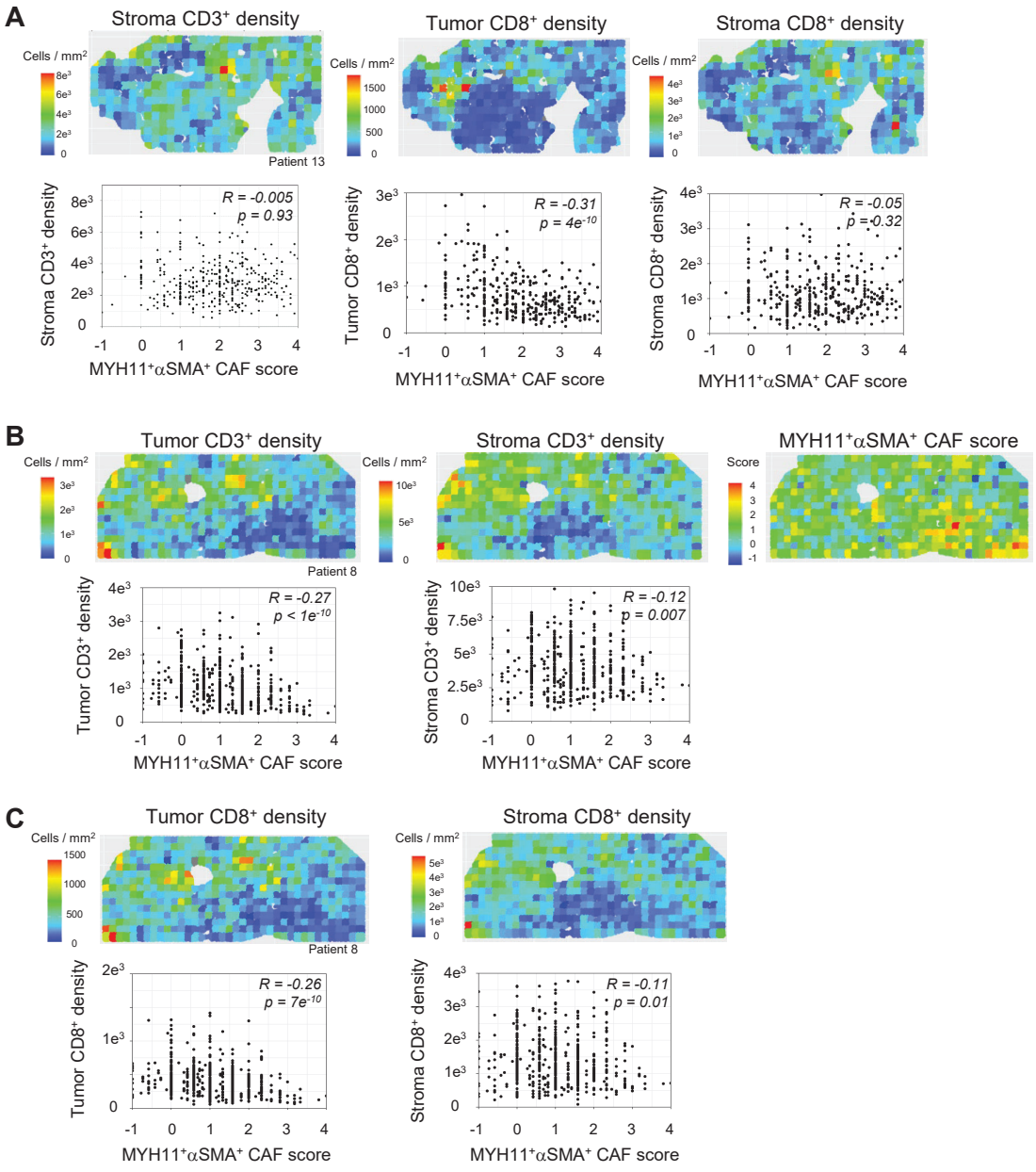

Supplemental fig. 10 (related to fig. 5) | A, Heatmaps of $CD3^+$ cell density in the stroma and $CD8^+$ cell density in the tumor and stroma of the patient 13. Respective dot plots and correlation (Pearson) with $MYH11^+\alpha SMA^+$ CAF score shown below each heatmap. **B**, $MYH11^+\alpha SMA^+$ CAF score, $CD3^+$ cell density heatmaps in the tumor and stroma of the patient 8. Dot plots of $CD3^+$ cell density correlation (Pearson) with $MYH11^+\alpha SMA^+$ CAF score shown below each heatmap. **C**, $CD8^+$ cell density in the tumor and stroma of the patient 8. Dot plots of $CD8^+$ cell density correlation (Pearson) with $MYH11^+\alpha SMA^+$ CAF score shown below each heatmap.

Figure S11, associated with figure 6

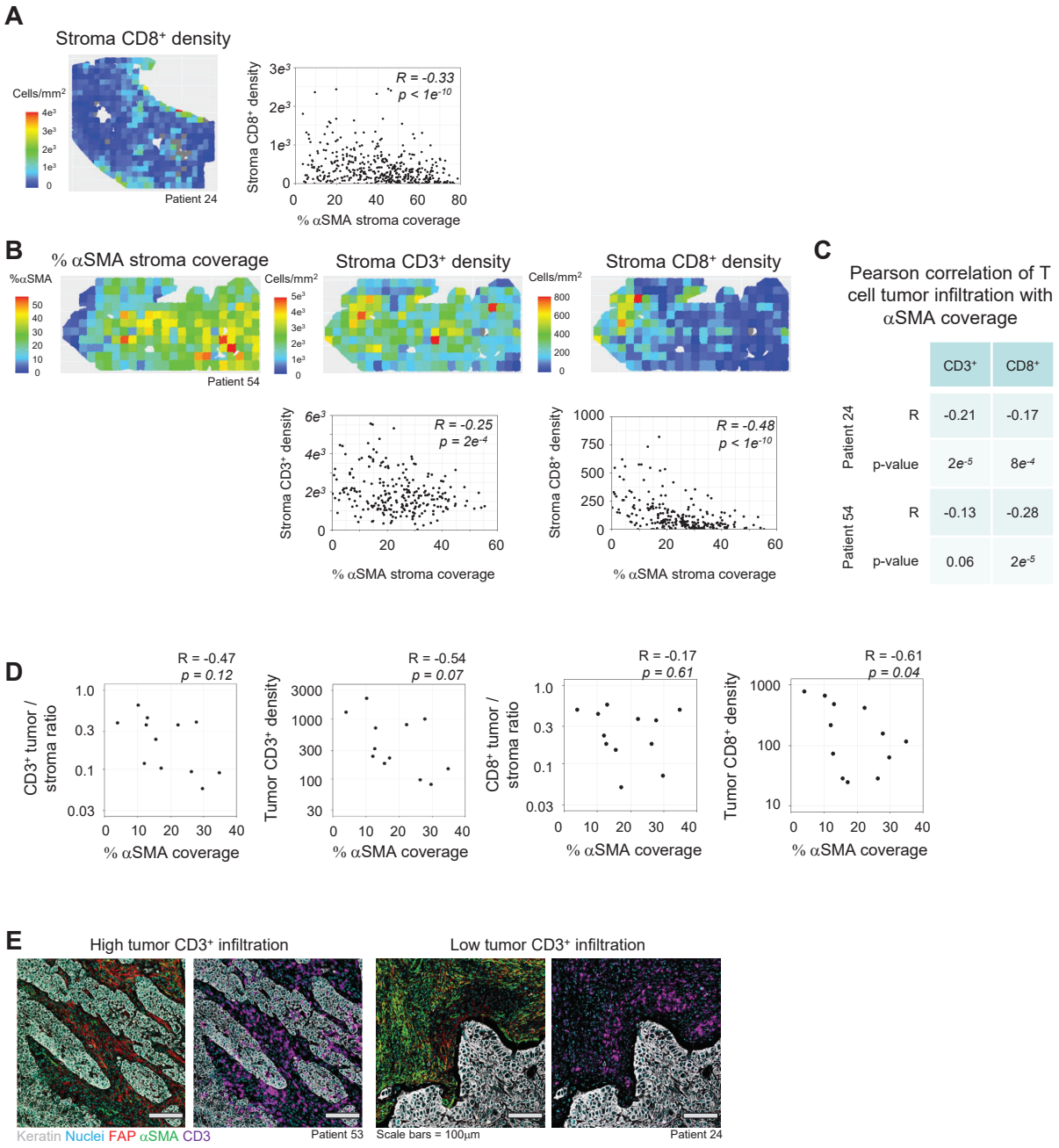

Supplemental fig. 11 (related to fig. 6) | A, Stroma $CD8^+$ cell density heatmap of patient 24 (left panel) and corresponding correlation (Pearson) dot plot with αSMA stroma coverage (right panel). **B**, αSMA coverage, stroma $CD3^+$ and $CD8^+$ cell density heatmap of the patient 54 (top panels) and corresponding correlation (Pearson) dot plots of $CD3^+$ and $CD8^+$ cell density with αSMA stroma coverage (bottom panels). **C**, Correlation (Pearson) of $CD3^+$ and $CD8^+$ cell tumor infiltration with stroma αSMA coverage in patients 24 and 54. **D**, Comparison of αSMA stroma coverage with $CD3^+$ and $CD8^+$ cell tumor infiltration for each patient. αSMA coverage and tumor infiltration is quantified across the entire tumor lesion. **E**, Example tumor lesions displaying high or low $CD3^+$ cell infiltration.

Figure S12, associated with figure 6

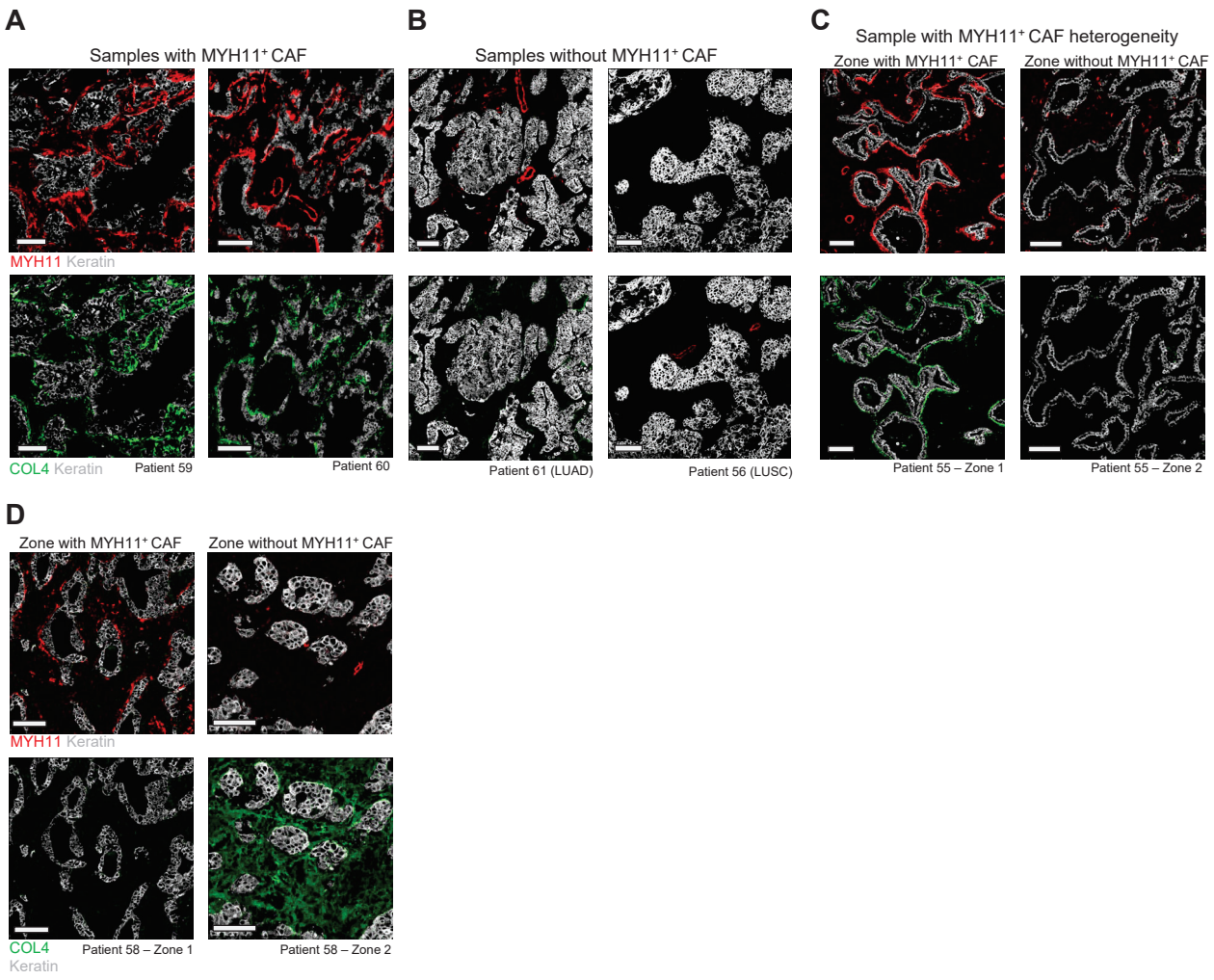

Supplemental fig. 12 (related to fig. 6) | A & B, Collagen IV is regularly found associated with $MYH11^{+}\alpha SMA^{+}$ CAF and not present when $MYH11^{+}\alpha SMA^{+}$ CAF do not exist. **C**, In samples with heterogenous $MYH11^{+}\alpha SMA^{+}$ CAF coverage, collagen IV is also found associated only in the regions with $MYH11^{+}\alpha SMA^{+}$ CAF. **D**, There are exceptions to these observations and collagen IV may be present without $MYH11^{+}\alpha SMA^{+}$ CAF or not present in $MYH11^{+}\alpha SMA^{+}$ CAF rich regions.

Figure S13, associated with figure 6

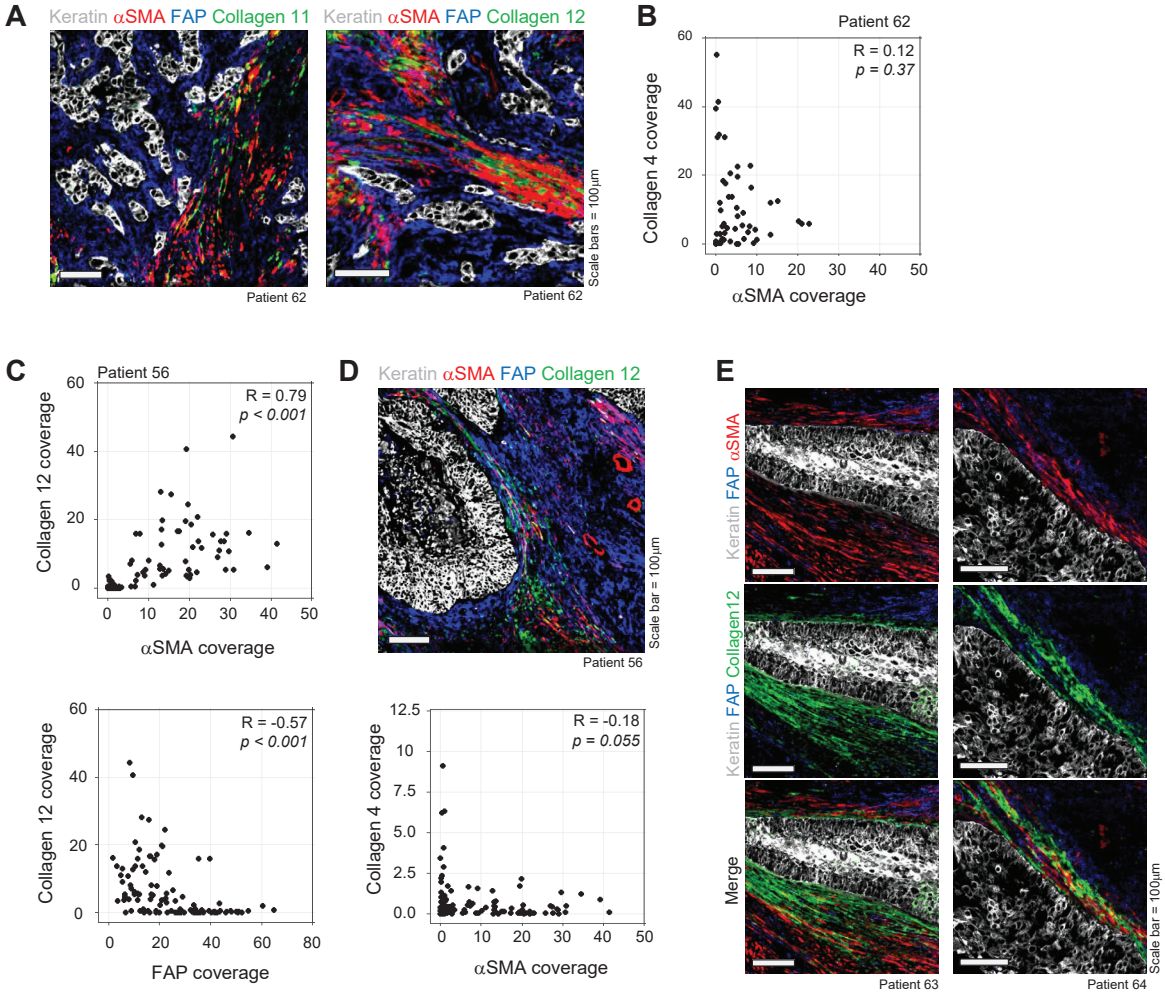

Supplemental fig. 13 (related to fig. 6) | A & B, $FAP^{+}\alpha SMA^{+}$ CAF co-stains with collagen XI and XII, (**B**) but not collagen IV, confirming the significant correlation quantified in figure 6E for patient 62. **C**, In an additional sample (patient 56), αSMA coverage of the stroma is significantly correlated (Spearman) with collagen XII deposition and not collagen IV, while FAP^{+} CAF show no correlation. Collagen XI staining was not detected in this tumor sample. **D**, Co-localization of collagen XII and αSMA in the tumor sample of patient 56. **E**, Additional representative examples showing collagen XII fibers colocalization with $FAP^{+}\alpha SMA^{+}$ CAF and their aligned organization.